# Remanence Evaluation Method in the Transformer Core Based on Magnetic Barkhausen Noise

Long Chen<sup>1,2,3</sup>, Long Wu<sup>1</sup>, Tong Ben<sup>3\*</sup>, and Hainan Huang<sup>1</sup>

<sup>1</sup>College of Electrical Engineering and New Energy, China Three Gorges University, Yichang 443002, Hubei Province, China 

<sup>2</sup>Hubei Provincial Research Center on Microgrid Engineering Technology (China Three Gorges University), 

Yichang 443002. Hubei Province. China

<sup>3</sup>Hubei Provincial Engineering Technology Research Center for Power Transmission Line, China Three Gorges University, Yichang, 443002, China

(Received 4 July 2025, Received in final form 9 September 2025, Accepted 9 September 2025)

As a consequence of the hysteresis phenomenon in transformer cores, an indeterminate remanence  $B_{\rm R}$  will persist in iron cores after the transformer is deactivated from the power grid. The remanence is the primary cause of inrush current during the no-load switching of transformers. Therefore, effectively evaluating transformer core remanence helps to suppress inrush current and enhance the power system's safe and stable operation. In this paper, a new remanence evaluation method based on Magnetic Barkhausen Noise (MBN) is proposed. Firstly, according to the J-A magnetization theory, a relationship between the peak voltage of MBN and the stress is obtained. Then, according to the magnetism model, a relationship between the stress and the remanence is established. Finally, based on the above relationship, the relationship between the peak voltage of MBN and the remanence is derived by using the stress as an intermediate quantity. In addition, an experimental platform based on a square iron core is used to examine the reliability of this approach in the paper. The obtained results indicate that the error of the proposed method is less than 6% in experiments. A novel theoretical framework for evaluating remanence is established in this research, which can provide important scientific and theoretical value.

Keywords: remanence, Magnetic Barkhausen Noise (MBN), iron core

#### 1. Introduction

Due to the hysteresis phenomenon of transformer cores, the remanence remains in the core after the transformer is powered off. When a transformer is switched on under no-load conditions, the remanence will cause the inrush current that can be as high as 6-8 times the steady-state rated current of the transformer if the direction of the remanence is the same as that of the excitation magnetic field. The inrush current can cause relay protection to malfunction, resulting in a large-scale power outage [1]. Meanwhile, the inrush current contains abundant secondary harmonics, severely degrading grid quality and damaging power electronics in renewable energy systems [2]. The phase-controlled switching technique proves most effective among conventional inrush current mitigation methods.

When the remanence is known, the inrush current can even be completely suppressed by this technique [3]. Although this technique has great application value, obtaining the magnitude and direction of the remanence accurately in the iron core has become a technical bottleneck for its large-scale application. Therefore, the accurate evaluation of the remanence in the transformer core is particularly important.

In recent years, numerous methodologies for evaluating the remanence in transformer cores have been proposed. According to statistics from the International Council on Large Electric Systems (CIGRE), most of the remanence value of power transformers after circuit breaker tripping can reach 20%-70% of the saturation flux value in the iron core [4]. Additionally, by analyzing the residual magnetism of over 500 transformers, it can be found that the remanence is mostly 0.7 times the rated magnetic flux density [5]. Based on the empirical estimation, this approach can offer a valuable reference for transformer manufacturers during factory testing of transformers.

©The Korean Magnetics Society. All rights reserved.

\*Corresponding author: Tel: +86 13820296113

e-mail: bentong@ctgu.edu.cn

However, this methodology is inherently incapable of yielding precise remanence values. The remanence value can be derived through the collection of induction voltage values at the instant of transformer switching [6]. This methodology is currently widely adopted due to its requirement for quantifying only a restricted set of parameters, specifically the circuit breaker operation time and inductive voltage. Nevertheless, its detection inaccuracies typically exceed 10% because its precision is influenced by multiple factors, including circuit breaker actuation time, magnetic leakage, winding leakage capacitance, and interception characteristics. In Ref. [7], by applying a DC voltage with changing polarity to the winding, the core is brought to saturation points in both the positive and negative directions. A partial saturation hysteresis loop of the core is depicted by recording the voltage and current waveforms throughout the process, and the remanence and residual coefficient of the iron core are calculated based on the obtained hysteresis loop. However, the proposed methodology is only operable under the prerequisite that the remanence orientation has been predetermined. In fact, since the remanence direction remains unknown in real-world engineering scenarios, the practical applicability of this method is inherently constrained. A magnetic flux sensor is employed to drive the remanence values by measuring the leakage magnetic field [8]. The accuracy of this methodology is constrained by the installation location of the sensor, and its applicability is restricted to transformers without oil tanks. Thus, there is currently no practical method for directly measuring remanence.

At present, various indirect methods for evaluating remanence are proposed. After applying DC excitation to the iron core, data on relevant physical quantities in the iron core under different remanence values are obtained, which are used to fit an empirical formula for calculating the remanence. The determination of remanence is achieved by establishing its dependency on the magnetizing current [9]. However, this approach only takes into account the positive transient currents during remanence formation, resulting in an incomplete consideration of the derived remanence calculation formula. Since remanence correlates not only with positive transient currents but also with negative ones. In Ref. [10], to further enhance this methodology, a novel remanence evaluation approach is proposed based on an analysis of the relationship between remanence and the difference in positive and negative transient currents. Nevertheless, this may result in reduced accuracy due to the difficulty in determining the measurement timing of transient current differences. In Ref. [11-15], the empirical formulas between remanence and other physical variables, including time constant, magnetizing inductance, energy, voltage-current phase angle difference, and response current waveform deviation degree, are established by the Finite Element Analysis (FEA). However, the empirical formula-fitting methodology suffers from severe limitations in generality. This approach is constrained by the simulation accuracy of Finite Element Analysis (FEA). Meanwhile, owing to the absence of explicit underlying physical significance, for different transformer cores, empirical formulas of remanence calculation must be redetermined through re-simulation, implying that the generalized migration capability of this methodology remains questionable. Based on the analysis of the above remanence evaluation methods, it can be found that there are still many problems with the current remanence evaluation in transformer cores. Therefore, it is still necessary to explore new remanence evaluation methods.

Over the past few decades, with the continuous development and advancement of electromagnetic theory, such as Alessandro-Beatrice-Bertotti-Montorsi (ABBM) magnetic domain theory [16], Jiles-Atherton (J-A) magnetization theory [17], and the Kypris-Jiles theory developed in recent years based on the J-A theory [18], as well as advancements in sensor material technology and manufacturing capabilities, signal processing technology, and computer analysis capabilities, the development of MBN signal technology has been relatively rapid. MBN signals are closely related to the microstructure, stress state, toughness, hardness, and other properties of materials, and their measurement has the characteristic of being non-destructive. In addition, the MBN signal also exhibits good sensitivity to deep defects and stress concentration in metallic materials, making it widely applied in non-destructive testing and characterization analysis of materials. For electrical equipment, including motors and transformers constructed from soft magnetic materials, MBN signals can be used to detect information such as the residual stress state and microstructural changes of these devices [19], enabling quick and easy assessment of their operating status. Considering that the MBN signals generation mechanism is similar to that of the remanence  $B_R$ , both of which are related to irreversible magnetic domain motion [17], the application of MBN signals for remanence detection has a great application prospect.

In this paper, a new method based on the MBN for the remanence evaluation is proposed. Firstly, a relationship between the remanence and the peak voltage of the MBN is established by using the stress as an intermediate physical quantity. Then, the direction of the remanence

can be determined by comparing the peak voltage of the MBN under the positive and negative remanence. Finally, the feasibility and accuracy of this method are verified with the square iron core, which is made of B30P105-type Grain Oriented (GO) silicon steels.

# 2. Remanence Evaluation Theory Based on MBN

### 2.1. Generation Mechanism of the Remanence and the MBN

The origins of the remanence and the MBN signals can be fundamentally attributed to the discontinuous and irreversible displacement of magnetic domain walls. The schematic diagram of the magnetic domain wall motion is shown in Fig. 1. Without the external magnetic field H, the domain wall resides at  $x_0$ , which is the minimum of the domain wall energy density  $\gamma(x)$ . At point  $x_0$ , because the first-order partial derivative and second-order partial derivative of the magnetic domain wall energy density with respect to its displacement x are 0 and greater than 0, respectively, the magnetic domain wall is in equilibrium and stable at  $x_0$ . When the magnetic field H is not 0, the magnetic domain wall starts to move. During the movement of the magnetic domain wall from  $x_0$  to  $x_1$ , if the magnetic field is removed, then the magnetic domain wall will follow the original path back to  $x_0$ , which is a reversible magnetization process. If the magnetic field continues to increase, the magnetic domain wall will pass through  $x_1$ . Because  $x_1$  is the point of maximum change of the magnetic domain wall energy density y(x), and the second-order partial derivative of the magnetic domain wall energy density concerning its displacement x is less

than 0 after  $x_1$ , the magnetic domain wall is in an unstable state, and it will cross all the points which are smaller than  $x_1$  and reside at  $x_3$ . If the magnetic field is removed at  $x_3$ , then the magnetic domain wall will not follow its original path back to  $x_0$ , but to  $x_2$ , which is an irreversible magnetization process. This indicates that the material retains a certain amount of remanence. In addition, in the irreversible magnetization process, the surface of the material releases continuous ultrasonic waves and continuous high-frequency pulsed voltages. This phenomenon is called the Magnetic Barkhausen Effect, and the resulting signals are called the MBN signals. From the above analysis of the generation Mechanism of the remanence and the MBN signals, it is evident that they are both related to the irreversible movement of domain walls. Therefore, the MBN signal and remanence are closely related, to the extent that the remanence level in the iron core can be characterized to a certain extent using the MBN signals.

# 2.2. Determination of the Remanence Direction Based on the Voltage of the MBN

The expression for the MBN signal activity can be expressed as [20]:

$$\frac{\mathrm{d}M_{\mathrm{JS}}}{\mathrm{d}t} = \frac{\mathrm{d}M_{\mathrm{irr}}}{\mathrm{d}H} \frac{\mathrm{d}H}{\mathrm{d}t} < M_{\mathrm{disc}} > \frac{\mathrm{d}N_{\mathrm{t}}}{\mathrm{d}M_{\mathrm{irr}}} \tag{1}$$

Where  $M_{\rm JS}$  is the total MBN signal activity, t is time, H is the magnetic field,  $M_{\rm irr}$  is the irreversible magnetization, N is the number of Barkhausen events, and  $<M_{\rm disc}>$  is the average size of the Barkhausen event. According to the law of electromagnetic induction, the voltage of the MBN signal can be expressed as:

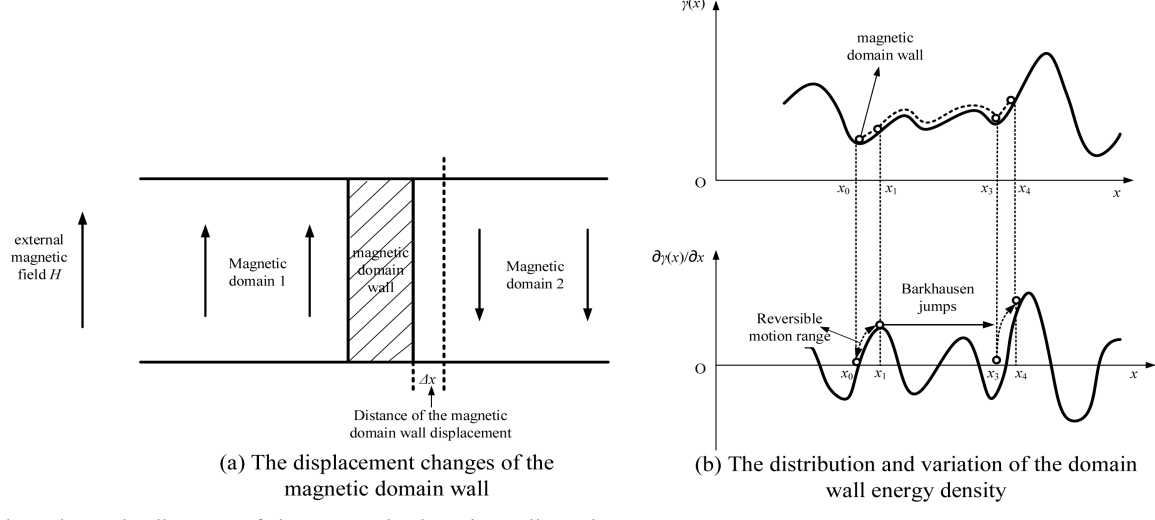


Fig. 1. The schematic diagram of the magnetic domain wall motion.

$$V_{\rm MBN} = -\mu_0 nS \frac{\mathrm{d}M_{\rm irr}}{\mathrm{d}H} \frac{\mathrm{d}H}{\mathrm{d}t} < M_{\rm disc} > \frac{\mathrm{d}N_{\rm t}}{\mathrm{d}M_{\rm irr}} \tag{2}$$

Where  $V_{\rm MBN}$  is the voltage signal of the MBN, n is the number of turns, S is the coil cross-sectional area, and  $\mu_0$  is the vacuum permeability. According to Eq. (2), it can be expressed as:

$$\max(\frac{\mathrm{d}M_{\mathrm{irr}}}{\mathrm{d}H}) \propto \max(\frac{\mathrm{d}M_{\mathrm{JS}}}{\mathrm{d}t}) \propto V_{\mathrm{MBN,peak}}$$
 (3)

In addition, the relationship between  $M_{\rm an}$  and  $M_{\rm irr}$  can be characterized as follows [21]:

$$M_{\rm irr} = \frac{M - c \bullet M_{\rm an}}{1 - c} \tag{4}$$

Where c is the reversible magnetization factor and  $M_{\rm an}$  is the anhysteretic magnetization.

When there exists a remanence, the magnetization M can be calculated as:

$$M = M_{\rm ac} + M_{\rm R} \tag{5}$$

Where  $M_{ac}$  is the magnetization under AC excitation and  $M_{R}$  is the residual magnetization.

Then, the  $M_{irr}$  can be divided into an AC magnetization acting part and a residual magnetization acting part by combining Eq. (4) with Eq. (5), which can be expressed:

$$M_{\rm irr} = \frac{M_{\rm ac} - c \bullet M_{\rm an}}{1 - c} + \frac{M_{\rm R}}{1 - c} \tag{6}$$

According to Eq. (6), it can be further concluded that the  $M_{\rm irr}$  can be classified into positive residual magnetization action and negative residual magnetization action:

$$\begin{cases}
M_{\text{irr}}^{+} = \frac{M_{\text{ac}} - cM_{\text{an}}}{1 - c} + \frac{M_{\text{R}}}{1 - c} \\
M_{\text{irr}}^{-} = \frac{M_{\text{ac}} - cM_{\text{an}}}{1 - c} - \frac{M_{\text{R}}}{1 - c}
\end{cases}$$
(7)

Where  $M_{\text{irr}}^{\dagger}$  and  $M_{\text{irr}}$  are the irreversible magnetization under positive and negative residual magnetization action, respectively. According to Eq. (7), it can be seen that  $M_{\text{irr}}^{\dagger} > M_{\text{irr}}$ 

In addition, the irreversible differential magnetization can be stated as [22]:

$$\frac{\mathrm{d}M_{\mathrm{irr}}}{\mathrm{d}H} = \frac{M_{\mathrm{an}}(H) - M_{\mathrm{irr}}(H)}{k\delta - \alpha(M_{\mathrm{an}}(H) - M_{\mathrm{irr}}(H))} \tag{8}$$

Where k is the pinning point parameter,  $\delta$  is the direction coefficient that is +1 at dH/dt > 0 otherwise -1,  $\alpha$  is the coupled mean-field parameter inside the magnetic

domains, and H is the magnetic field strength.

According to Eq. (8), the following result can be introduced:

$$\frac{dM_{irr}^{+}}{dH} < \frac{dM_{irr}^{-}}{dH} \Rightarrow \max(\frac{dM_{irr}^{+}}{dH}) < \max(\frac{dM_{irr}^{-}}{dH})$$
 (9)

According to Eq. (3) and Eq. (9), the relationship between the peak voltage of the MBN under the action of positive and negative residual magnetization is finally derived:

$$V_{\text{MBN,peak}}^{+M_{\text{R}}} < V_{\text{MBN,peak}}^{-M_{\text{R}}} \tag{10}$$

Based on Eq. (10), it is concluded that the peak voltage amplitude of the MBN is reduced under the positive remanence compared to its negative counterpart, and this phenomenon can be used to make a judgment on the direction of the remanence.

## 2.3. Construction of the Relationship between the Remanence and the Peak Voltage Signal of the MBN

Considering that the MBN signal generation mechanism is similar to that of the remanence  $B_R$ , both of which are related to irreversible domain wall motion, and that the magnetic domains are affected by the stress in the material, the relationship between the peak voltage of the MBN and the remanence is established by using the stress as an intermediate physical quantity.

Firstly, the relationship between the peak voltage of the MBN and the stress is constructed. In the absence of an external magnetic field, when only stress is present, the ferromagnetic material satisfies the following [23, 24]:

$$\chi_{\text{max}}^{'}(\sigma)|_{H=0} = \frac{M_{\text{s}}}{3a - (\alpha + 3b\sigma / \mu_0)M_{\text{s}}}$$
 (11)

Where  $\sigma$  is the stress,  $M_s$  is the saturation magnetization, and b is the proportional coefficient.

According to Eq. (11), it can be further deduced:

$$\frac{1}{\chi_{\text{max}}(0)|_{H=0}} - \frac{1}{\chi_{\text{max}}(\sigma)|_{H=0}} = \frac{3b\sigma}{\mu_0}$$
 (12)

Where  $\chi'_{\text{max}}(0)$  and  $\chi'_{\text{max}}(\sigma)$  are the differentials of the maximum magnetization of ferromagnetic materials without and with stress, respectively.

The peak voltage of the MBN is directly proportional to the  $\chi'_{\text{max}}(\sigma)$  intensity [23]. According to Eq. (12), it can be obtained:

$$\frac{1}{V_{\text{MBN,peak}(0)}} - \frac{1}{V_{\text{MBN,peak}(\sigma)}} = \frac{3b'\sigma}{\mu_0}$$
 (13)

Where b' is the proportional coefficient.  $V_{\text{MBN,peak}(0)}$  and  $V_{\text{MBN,peak}(\sigma)}$  are the peak voltage of the MBN without and with the stress.

Then, the relationship between the residual magnetization and the stress is established. The stress and material properties determine the magnitude of coercivity, and the critical magnetic field is also determined by the stress and material properties. The coercivity is proportional to the critical magnetic field, then the coercivity can be expressed as:

$$H_{\rm C} = pH_0 \tag{14}$$

Where p is a constant factor with a maximum value of 1.  $H_{\rm C}$  and  $H_0$  are the coercivity and critical magnetic fields, respectively.

Since the stress distribution varies among the individual grains of the polycrystalline structure, the magnitude of  $H_0$  differs across different regions. Substituting the steady-state value of  $H_0$  into equation (14),  $H_C$  can be approximately expressed as [25]:

$$H_{\rm C} \approx p \frac{3\lambda_{\rm S}\sigma}{2\mu_{\rm o}M_{\rm S}} \tag{15}$$

Where  $\lambda_s$  is the magnetostriction.

Assuming the magnetic domain is modeled as a prolate spheroid with semi-major axis a and semi-minor axis b (a > b), when an external magnetic field H is applied along the a-axis, inducing a rotation of the magnetic moment, the angle of deviation of the magnetic moment from the a-axis is denoted as  $\theta$ . Consequently, the magnetic energy can be expressed as:

$$E_{\rm H} = -\mu_0 M_{\rm S} H \cos(\pi - \theta) = \mu_0 M_{\rm S} H \cos \theta \tag{16}$$

Where  $E_{\rm H}$  is the magnetic energy.

Since the magnetic moment has two components,  $M_a$  along the a-axis and  $M_b$  along the b-axis, let  $N_1$  and  $N_2$  denote the demagnetization factors for the a-axis and b-axis, respectively. The demagnetization energy can be expressed as:

$$E_{\rm d} = \frac{\mu_0 M_{\rm S}^2}{2} (N_1 \cos^2 \theta + N_2 \sin^2 \theta)$$
 (17)

The total energy of the magnetic domain can be expressed as:

$$E = E_H + E_J \tag{18}$$

According to Eq. (18), the critical magnetic field is obtained as:

$$H_0 = M_S(N_2 - N_1) \tag{19}$$

For a polycrystal, the long axes of the individual grains are oriented differently, resulting in:

$$H_{\rm C} = pAM_{\rm S}(N_2 - N_1) \tag{20}$$

Where A is the average factor, and it can be obtained by using the average effect.

For cubic crystals, by using spherical coordinates, the residual magnetization  $M_{\rm R}$  of single-axis anisotropic micrograms in a disordered state can be calculated as:

$$M_{\rm R} = 0.866 M_{\rm S} \tag{21}$$

According to Eq. (15), Eq. (20) and Eq. (21), the residual magnetization can be expressed as:

$$M_{\rm R} = \sqrt{p \frac{3\lambda_{\rm S}\sigma}{2\mu_0 A(N_2 - N_1)}}$$
 (22)

Finally, according to Eq. (13) and Eq. (22), the relationship between the residual magnetization and the peak voltage of the MBN can be obtained:

$$M_{\rm R} = \sqrt{p \frac{\lambda_{\rm S}}{2b' A(N_2 - N_1)} (\frac{1}{V_{\rm MBN,peak(0)}} - \frac{1}{V_{\rm MBN,peak(M_R)}})}$$
(23)

Where  $V_{\mathrm{MBN,peak}(0)}$  and  $V_{\mathrm{MBN,peak}(MR)}$  are the peak voltage of the MBN without and with the residual magnetization, respectively. In ferromagnetic materials, the magnetic flux density in the sample can be calculated as:

$$B = \mu_0(M+H) \tag{24}$$

When the external magnetic field is removed, the remanence  $B_R$  can be given by:

$$B_{\rm p} = \mu_0 M_{\rm p} \tag{25}$$

Combining Eq. (23) and Eq. (25), the relationship between the remanence  $B_R$  and the peak voltage is obtained:

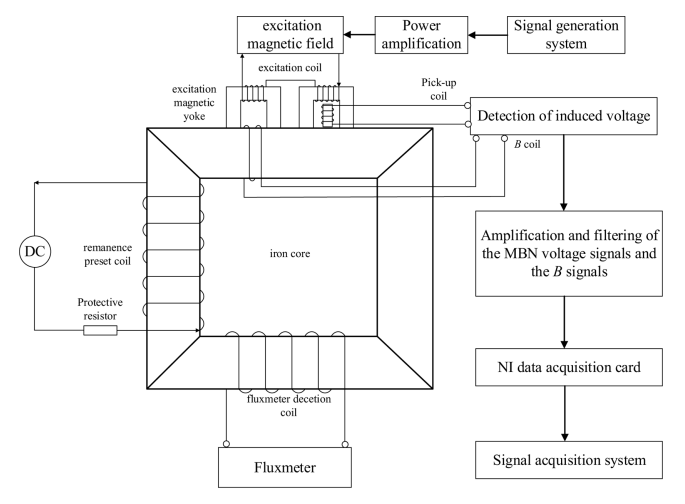
$$B_{\rm R} = \mu_0 \sqrt{p \frac{\lambda_{\rm S}}{2b' A(N_2 - N_1)}} \left(\frac{1}{V_{\rm MBN, peak(0)}} - \frac{1}{V_{\rm MBN, peak(B_{\rm R})}}\right)$$
(26)

When a given material is measured, the  $\lambda_S$ ,  $N_2$ ,  $N_1$ , p, b', and A can be regarded as constants. Therefore, the coefficient in the above equation before the MBN voltage is a constant. From this, the remanence  $B_R$  value can be obtained from the peak value of the measured MBN voltage signal.

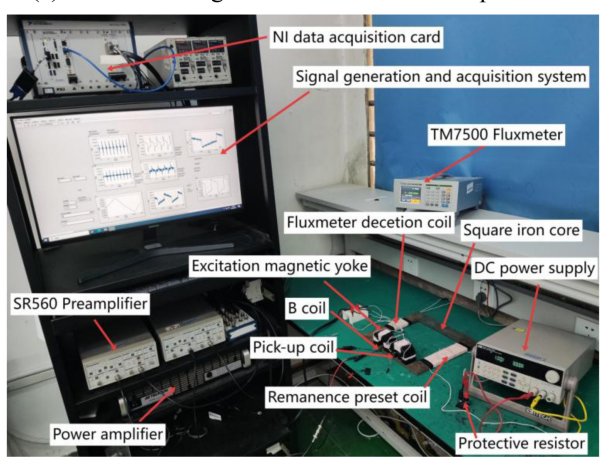
### 3. Experimental Verification

### 3.1. Establishment of an Experimental Platform

To verify the correctness of the remanence evaluation



(a) Schematic diagram of the measurement platform.



(b) Composition of experimental measuring devices.

Fig. 2. (Color online) The experimental measurement platform.

based on the MBN, an experimental platform of remanence detection based on the square iron core that has an effective cross-sectional area of 400 mm<sup>2</sup> and an effective magnetic circuit length of 960 mm is established in this paper. The experimental measurement platform is presented in Fig. 2. A fluxmeter is used to detect the precharging value of the remanence after applying different DC excitations to the iron core. Furthermore, to ensure the accuracy of the precharging value of the remanence in the experiment, the AC demagnetization method is used to carry out thorough demagnetization so that the initial remanence in the iron core is 0.

To detect the MBN signal in the iron core, firstly, the magnetization waveform is generated by the signal generation system and is delivered to the excitation coil so that the iron core can be magnetized by a U-shaped magnetic yoke. Subsequently, the voltage signal of the MBN is detected by a pickup coil placed on the surface of

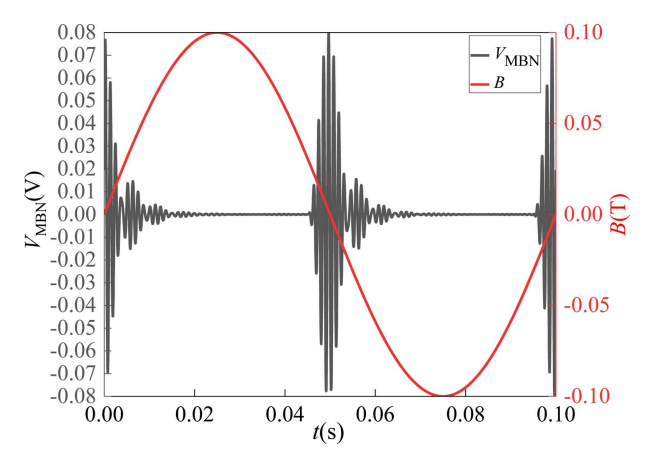


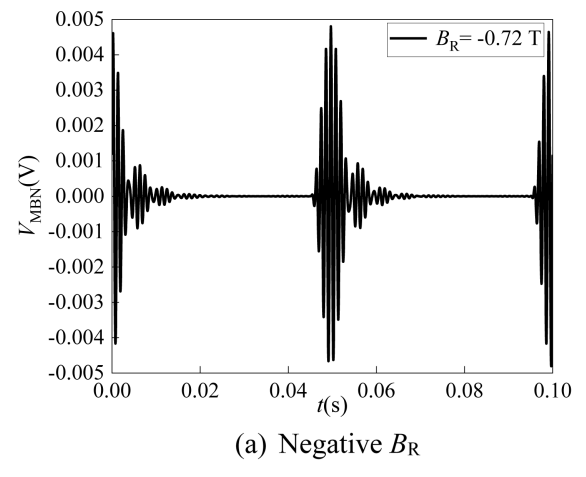
**Fig. 3.** (Color online) Relationship between magnetic flux density and MBN voltage signals.

the iron core. Finally, the acquired signals of the voltage, which are filtered and amplified, are transmitted to the acquisition system to obtain the voltage of the MBN by using LabVIEW software. At the same time, to ensure that the magnetic field applied during the measurement of the MBN signal does not pass through the entire iron core magnetic circuit, this paper uses a double magnetic yoke compensation method to cancel out the magnetic circuit in the entire iron core, so that the magnetic field only forms a circuit on one side of the iron core, thereby reducing the impact of the applied excitation on the original remanence in the entire iron core.

To verify the accuracy of the MBN signal detected in the iron core, the magnetic flux density B is also measured by using the B coil in this paper. The MBN signal and magnetic flux density waveform diagram under one magnetization cycle are shown in Fig. 3. According to the property that the MBN signal mostly occurs at the coercive point of the hysteresis loop, and the magnetic density B at the coercive point is 0. As can be seen from Fig. 3, the location where the MBN signal occurs is exactly the location where the magnetic density is 0. The above theoretical analysis shows that the MBN signal obtained from the simulation is reasonable.

#### 3.2. Results and Discussion

To minimize the impact of the original remanence in the iron core during the remanence evaluation process and ensure that a good voltage signal of the MBN can be obtained, an alternating voltage of 0.25 V that is used as the excitation voltage is applied to the U-shaped magnetic yoke in this paper. On the other hand, the direction of remanence must also be known during the remanence detection process. To determine the directionality of the remanence, the positive and negative remanence are



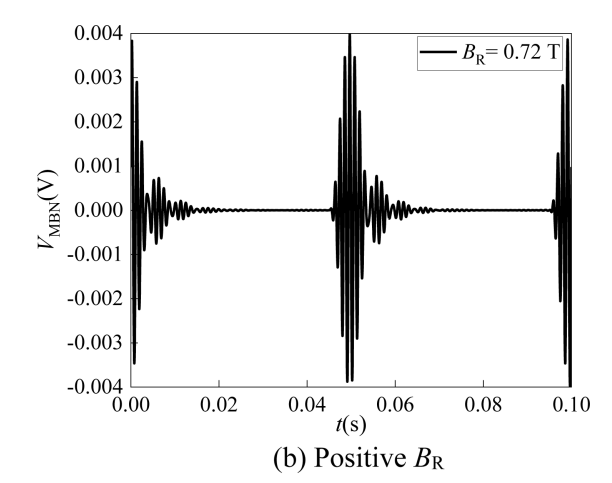


**Fig. 4.** The voltage of the MBN under different direction of  $B_R$ .

precharged by adjusting the polarity of the DC voltage. Then, the voltage peak of the MBN corresponding to the positive and negative remanence is collected in Fig. 4. As shown in Fig. 4, the voltage peak value is different when the remanence direction is different.

From Fig. 4, it can be found that when the applied AC excitation's initial direction is consistent with the remanence direction, the voltage peak value of the MBN is low. Conversely, if the starting direction of the applied AC excitation is reversed relative to the remanent is opposite to the direction of the remanence, the voltage peak value of the MBN is high. According to this phenomenon, when the applied excitation is determined, the voltage peak value of the MBN under positive and

negative remanence can be used to judge the positive and negative direction of the detected remanence.

To further realize the evaluation of the specific value of the remanence, the experimental procedure for remanence evaluation is established in Fig. 5. The experimental procedure is divided into the determination of formula parameters and the remanence evaluation process.

Firstly, because the  $\mu_0$ ,  $\lambda_S$ ,  $N_2$ ,  $N_1$ , p, b', and A are constants in Eq. (26), the Eq. (26) can be further simplified as follows:

$$B_{\rm R} = \sqrt{\frac{X}{V_{\rm MBN,peak(B_{\rm R})}} + Y} \tag{27}$$

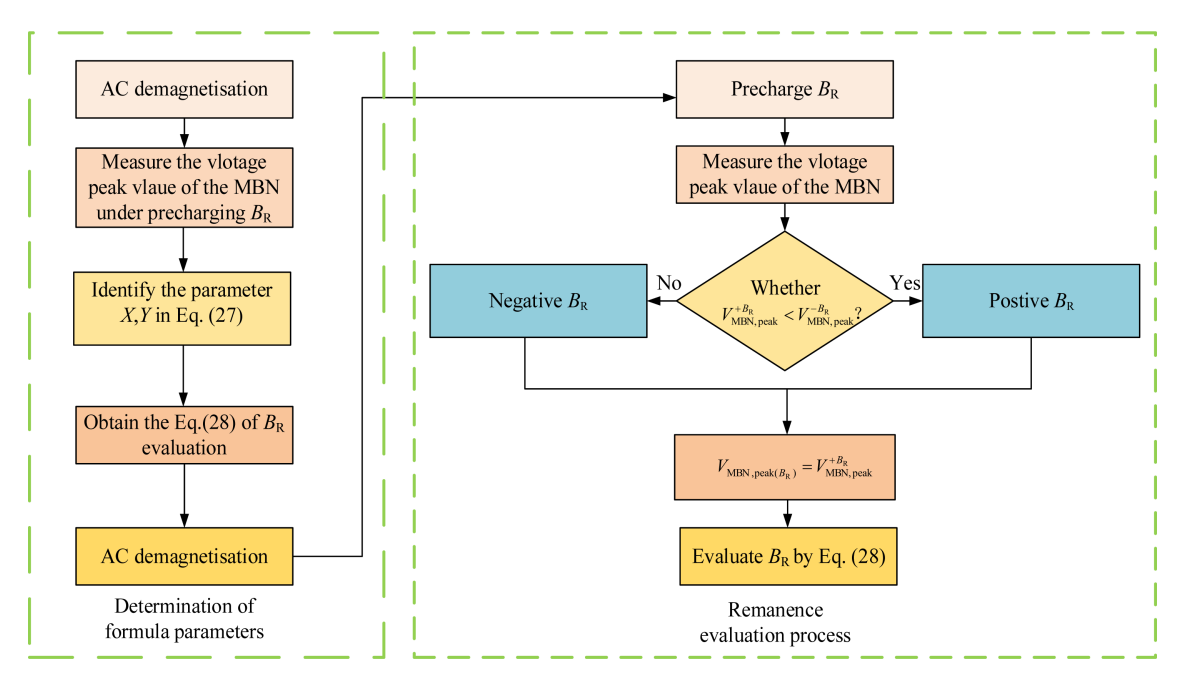
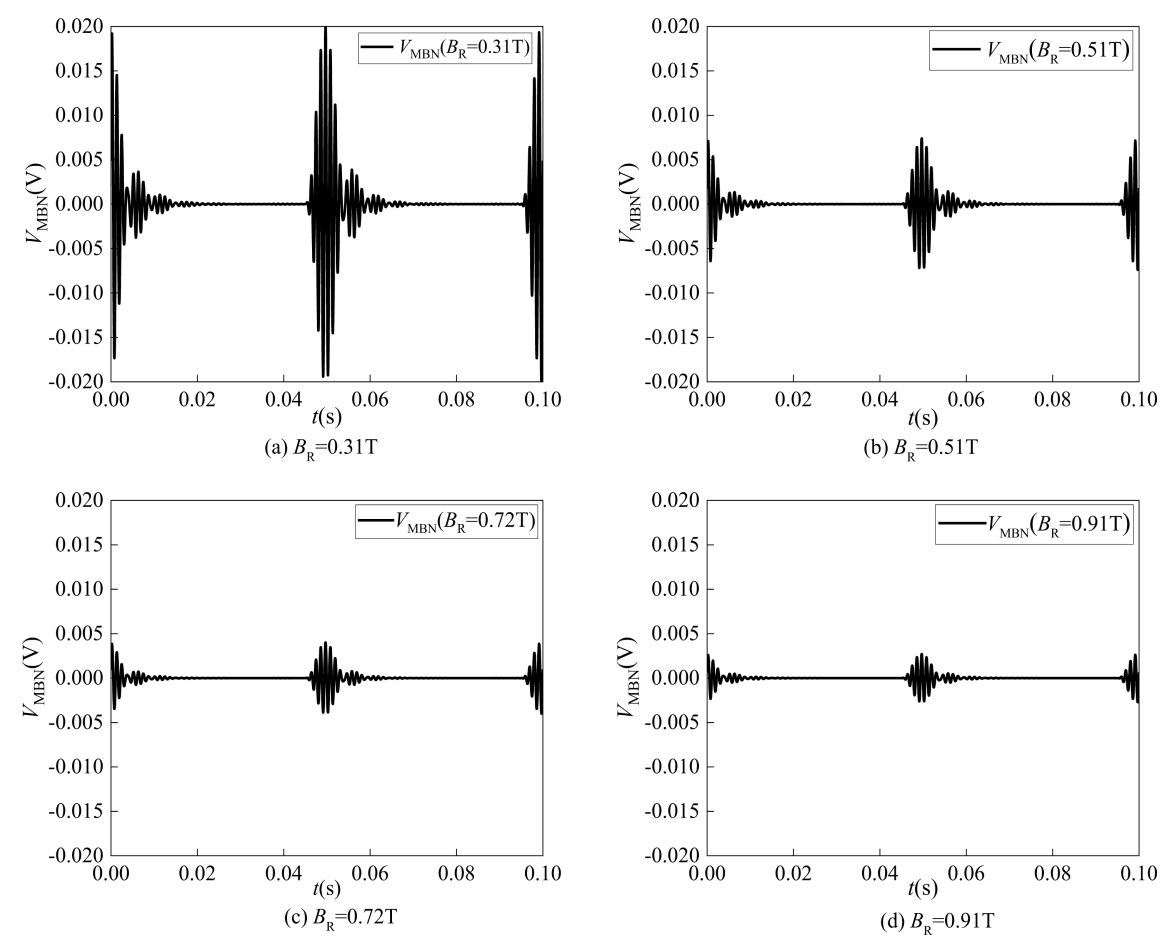


Fig. 5. (Color online) Experimental procedure for remanence evaluation.



**Fig. 6.** The voltage signal of the MBN in different  $B_R$  levels.

To more accurately determine the parameters X and Y in Eq. (27), the Root-Mean-Square Error (RMSE) between the remanence values computed by Eq. (27) and the experimentally precharging remanence values is adopted as the objective function. Through optimization algorithms, Eq. (27) can ultimately be expressed as:

$$B_{\rm R} = \sqrt{\frac{2.286 \times 10^{-3}}{V_{\rm MBN,peak(B_{\rm R})}} + 0.029}$$
 (28)

Finally, the remanence can be calculated by Eq. (28). At the same time, the positive and negative directions of the remanence can be determined by the magnitude of the voltage peak value of the MBN.

Since the remanence value is the same in positive and negative directions, in this paper, different positive remanence values are preset, and the voltage of the MBN at the different remanence values is measured in Fig. 6. As can be clearly observed from Fig. 6, the voltage of the MBN signal gradually decreases with increasing remanence. In this paper, the peak voltage of the MBN signal is

**Table 1.** The peak voltage of MBN under the different precharging remanence  $B_R$ .

Precharging $B_{R}(T)$	$V_{\mathrm{MBN,peak}(BR)}\!(\mathrm{V})$
0.31	0.0200
0.42	0.0122
0.51	0.0074
0.61	0.0054
0.72	0.0040
0.81	0.0034
0.91	0.0027

extracted in Table 1.

For enhanced visualization of the connection between the peak voltage of the MBN signal and the remanence, they are plotted in Fig. 7. As can be seen from Fig. 7, as the precharging remanence increases, the intensity of the detected MBN peak voltage signal gradually weakens in the experiment. There is a nonlinear inverse relationship between the MBN peak voltage signal and the remanence

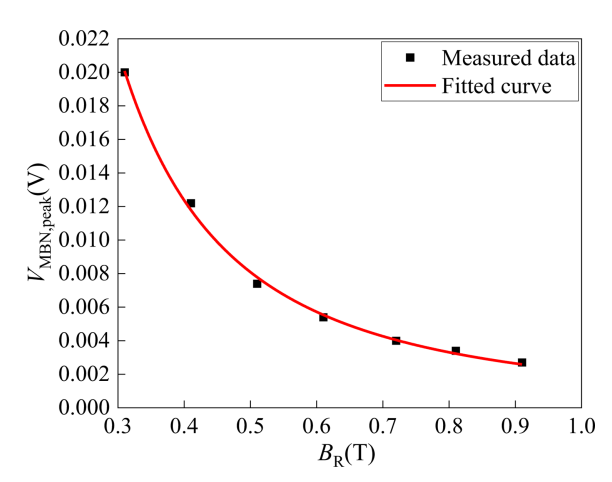


**Fig. 7.** (Color online) Relationship between the  $B_R$  and the  $V_{\text{MBN,peak}(B_R)}$ .

from the fitted curve in Fig. 1. At the same time, this trend is consistent with the relationship between the peak voltage of the MBN and remanence established by Eq. (28).

To further demonstrate the reliability and practicality of Eq. (28), the relative error between the precharging remanence values and the remanence values calculated by using Eq. (28) is presented as follows:

$$\varepsilon\% = \frac{|B_{\rm Rm} - B_{\rm Rc}|}{B_{\rm Rm}} \bullet 100\% \tag{29}$$

Where  $B_{\rm Rm}$  is the experimental precharging remanence value, and  $B_{\rm Rc}$  is the remanence value calculated using Eq. (28).

The comparison results between the experimentally measured precharging remanence and the remanence

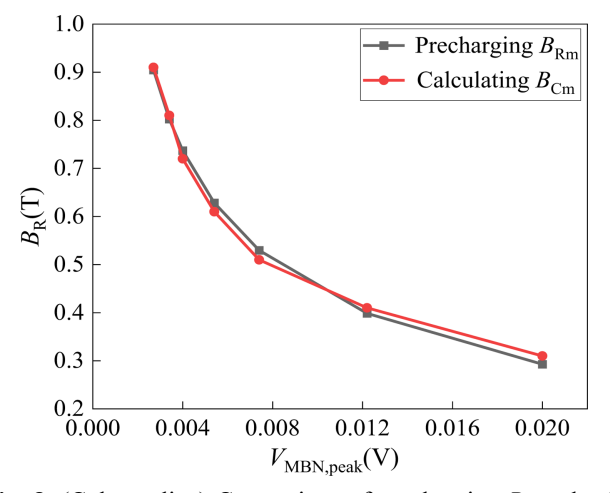


**Fig. 8.** (Color online) Comparison of precharging  $B_R$  and calculated  $B_R$ .

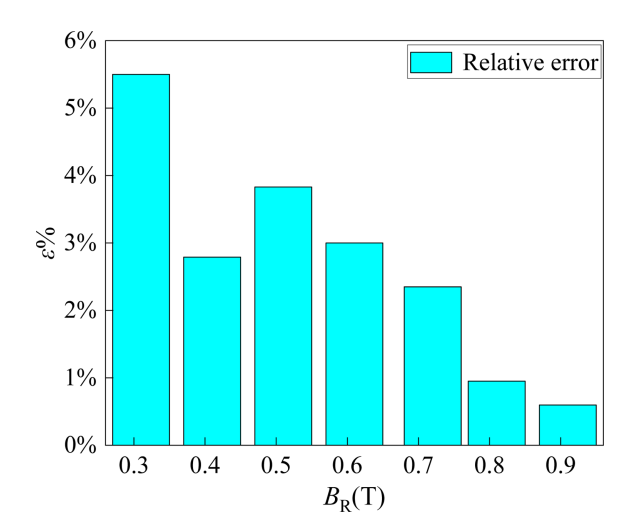


**Fig. 9.** (Color online) Error distributions under different levels of  $B_R$ .

calculated by the peak voltage of the MBN are presented in Fig. 8. As shown in Fig. 8, it can be clearly observed that the remanence values calculated based on the peak voltage of the MBN show a high degree of consistency with the experimentally precharging remanence values, particularly when the residual magnetism in the iron core exceeds 0.7 T. Meanwhile, the error distributions under different levels of  $B_R$  are also shown in Fig. 9. It can be seen that when the remanence value is higher in the core, the error is lower, and the effect of this method is better in Fig. 9. The obtained results indicate that the maximum relative error magnitude between the experimentally precharging remanence and the calculated remanence is less than 6%, significantly outperforming the voltage integration method reported in Ref. [26]. Notably, when the remanence exceeds 0.4 T, the error can be minimized to below 5%, indicating that the precision of the proposed approach in this study is commensurate with the latest developments in remanence detection methods [27]. However, the method proposed in Ref. [27] relies on empirical formula fitting and requires the re-determination of the fitting coefficients for different transformer cores. This is attributed to its absence of explicit underlying physical interpretation. Nevertheless, the proposed method in this paper not only exhibits explicit physical interpretability but also ensures a high level of accuracy.

#### 4. Conclusion

An innovative approach for remanence evaluation based on the peak voltage of the MBN is introduced in the present research. The relationship between the peak voltage of the MBN and the remanence is constructed by

using the stress as an intermediate physical quantity. The direction of the remanence can be inferred by comparing the peak voltage of the MBN under the positive and negative remanence. The results show that the peak voltage of the MBN exhibits a decreasing trend with increasing remanence in the core. Notably, the amplitude of the MBN peak voltage is markedly suppressed under positive remanence when compared to negative remanence conditions. The outcomes illustrate that the error of the presented approach is less than 6%. The proposed methodology enhances the theoretical basis for remanence detection by virtue of its capability to exhibit explicit physical interpretability. At present, due to limitations in experimental equipment, the relationship for the remanence evaluation is initially established by using stress as an intermediate physical quantity in this paper. However, practical applications must also account for other factors that may influence the remanence evaluation based on the MBN signal. The multi-factor coupling impact analysis will be further researched in the future.

### Acknowledgment

This work was supported by the National Natural Science Foundation of China under Grant No. 52477011, 52207012.

### References

- [1] Y. Z. Gerdroodbari, M. Davarpanah, and S. Farhangi, IEEE Trans. Power Del. **33**, 2938 (2018).
- [2] S. F. Chou, C. T. Lee, H. C. Ko, and P. T. Cheng, IEEE Trans. Power Electr. **29**, 1710 (2014).
- [3] J. Mitra, X. Xu, and M. Benidris, IEEE Trans. Ind. Appl. **56**, 890 (2020).
- [4] Y. F. Wu, H. R. Hu, W. Luo, T. Wang, and L. Ruan, Asia-Pacific Power and Energy Engineering Conference, IEEE Computer Society (2011) pp.37-39.
- [5] E. Colombo and G. Santagostino, Electra. 94, 35 (1984).
- [6] S. Q. Zhang, S. Y. Shun, G. Li, K. Wang, J. Z. Li, and J. Y. Lui, High Voltage Eng. 47, 732 (2021).

- [7] T. Liu, X. Liu, S. B. Liang, J. K. Wang, and C. G. Rao, Trans. China Electrotech. Soc. 32, 137 (2017).
- [8] D. Cavallera, V. Oiring, J. L. Coulomb, O. Chadebec, B. Caillault, and F. Zgainski, IEEE Trans. Magn. 50, 7024904 (2014).
- [9] W. Q. Ge, Y. H. Wang, Z. H. Zhao, X. G. Yang, and Y. J. Li, IEEE Trans. Appl. Supercond. 24, 0502404 (2014).
- [10] C. L. Huo, Y. H. Wang, Z. W. Zhao, and C. C. Liu, IEEE Trans. Appl. Supercond. 30, 5500505 (2020).
- [11] C. L. Huo, Y. H. Wang, S. P. Wu, Y. M. Yang, and Z. W. Zhao, IEEE Trans. Magn. 57, 8400204 (2021).
- [12] C. L. Huo, Y. H. Wang, C. C. Lui, and G. Lei, IET Electr. Power Appl. **16**, 224 (2022).
- [13] C. L. Huo, Y. H. Wang, S. P. Wu, and C. C. Liu, IEEE Trans. Instrum. Meas. **70**, 6011909 (2021).
- [14] Y. Z. Ren, Y. H. Wang, C. C. Liu, and S. P. Wu, AIP Adv. 13, 025332 (2023).
- [15] Y. Z. Ren, Y. H. Wang, and C. C. Liu, J. Magn. Magn. Mater. 600, 172155 (2024).
- [16] B. Alessandro, C. Beatrice, G. Bertotti, and A. Montorsi, J. Appl. Phys. 68, 2901 (1990).
- [17] D. C. Jiles, Czech. J. Phys. **50**, 893 (2000).
- [18] O. Kypris, I. C. Nilebedim, and D. C. Jiles, IEEE Trans. Magn. 49, 3893 (2013).
- [19] J. A. Perez-Beniteza, J. Capo-Sancheza, J. Anglada-Rivera, and L. R. Padovese, J. Magn. Magn. Mater. 288, 433 (2005).
- [20] D. C. Jiles and W. Kiarie, IEEE Trans. Magn. 57, 800211 (2021).
- [21] N. Sadowski, N. J. Batistela, J. P. A. Bastos, and M. Lajoie-Mazenc, IEEE Trans. Magn. 38, 797 (2002).
- [22] D. Lederer, H. Igarashit, A. Kost, and T. Honmat, IEEE Trans. Magn. **35**, 1211 (1999).
- [23] L. Mierczak, D. C. Jiles, and G. Fantoni, IEEE Trans. Magn. 47, 459 (2011).
- [24] D. C. Jiles, D. L. Atherton, J. Magn. Magn. Mater. **61**, 48 (1986).
- [25] N. L. Schryer and L. R. Walker, J. Appl. Phys. 45, 5406 (1974).
- [26] C. L. Huo and Y. M. Yang, IEEE Sens. J. **24**, 7636 (2024).
- [27] C. L. Huo and Y. M. Yang, IEEE Sens. J. **24**, 2647 (2024).